Structure-Based Optimization of Peptide Inhibitors of Mammalian Ribonucleotide Reductase[†,‡]

Maria Pellegrini,[§,||,⊥] Sebastian Liehr,[⊥,#] Alison L. Fisher,[#,▽] Paul B. Laub,[▼,○] Barry S. Cooperman,[*,#] and Dale F. Mierke[*,§,●]

Department of Molecular Pharmacology, Division of Biology and Medicine, and Department of Chemistry, Brown University, Providence, Rhode Island 02912, Department of Chemistry, University of Pennsylvania, Philadelphia, Pennsylvania 19104, and Fox Chase Cancer Center, Philadelphia, Pennsylvania 19111

Received June 9, 2000

ABSTRACT: Mammalian ribonucleotide reductase (mRR), a potential target for cancer intervention, is composed of two subunits, mR1 and mR2, whose association is critical for enzyme activity. In this article we describe the structural features of the mRR-inhibitor Ac-F-c[ELAK]-DF (Peptide 3) while bound to the mR1 subunit as determined by transferred NOEs. Peptide 3 is a cyclic analogue of the *N*-acetylated form of the heptapeptide C-terminus of the mR2 subunit (Ac-FTLDADF), which is the link between the two subunits and previously shown to be the minimal sequence inhibitor mRR by competing with mR2 for binding to mR1. Structural refinement employing an ensemble-based, full-relaxation matrix approach resulted in two structures varying in the conformations of F^1 and the cyclic lactam side chains of E^2 and K^5. The remainder of the molecule, both backbone and side chains, is extremely well-defined, with an RMSD of 0.54 Å. The structural features of this conformationally constrained analogue provide unique insight into the requirements for binding to mR1, critical for further inhibitor development.

Mammalian ribonucleotide reductase (mRR)[1] catalyzes the radical deoxygenation of ribonucleotides to 2′-deoxyribonucleotides, which is the rate-determining step in de novo DNA synthesis (*1*). As such, it is a potential target for cancer intervention (*2*). The enzyme is composed of two different subunits, mR1 and mR2, with masses of 90 and 45 kDa, respectively. The larger mR1 subunit carries the substrate binding site as well as two allosteric sites while the smaller mR2 subunit contains two μ-oxygen-bridged high-spin Fe(III)s and a stable tyrosine radical. For turnover to occur, mR2 must bind to mR1, allowing an electron to be transferred between the tyrosine radical and the substrate site (*3*−*5*). This binding takes place via the C-terminal residues of mR2, and can be inhibited by peptides mimicking the C-terminal sequence of mR2 (*6*). The linear heptapeptide Ac-FTLDADF (Peptide 1), corresponding to the seven C-terminal amino acids of mR2, was found to have the minimum length necessary for full inhibitory activity (*7*).

Based on the structural features of this linear analogue (Peptide 1), and the closely related heptapeptide Ac-YTLDADF (Peptide 2), while bound to mR1, as determined by transferred nuclear Overhauser effects (NOEs) (*8*, *9*), a series of cyclic analogues, employing a lactam bridge between the side chains of residues 2 and 5, were synthesized and tested for binding affinity to mR1 (*10*). Variations of the length of these side chains, thereby altering the ring size, as well as the direction of the lactam amide bond, affect the inhibitory activity and are therefore significant variables in the design of mRR inhibitors (*10*). To obtain structural insight into these findings, we have undertaken the characterization of the conformational preferences of the most active cyclic analogue, Ac-F-c[ELDK]-DF (Peptide 3), while bound to mR1. This peptide, containing an 18-membered lactam ring, had superior (∼2.5-fold) binding and inhibitory activity toward mR1 and mRR, respectively, than Peptide 1. The structural features of this analogue, structurally constrained by the cyclization, provide important properties for the rational design of optimized inhibitors of mRR activity.

EXPERIMENTAL PROCEDURES

Sample Preparation. The preparation of the mR1 subunit of mRR was carried out following published procedures (*11*). Peptides 3−7 were synthesized and cyclized on solid-support,

[†] This work was supported in part by National Institutes of Health Grants GM-54082 (D.F.M.) and CA-58567 (B.S.C.), and by the Research Corporation through a Cottrell Scholars Award (D.F.M.).

[‡] Coordinates have been deposited in the Protein Data Bank (accession code 1foz).

* To whom correspondence should be addressed at the Department of Molecular Pharmacology, Division of Biology and Medicine, Brown University, Providence, RI 02912. Voice: (401)863-2139; Fax: (401)-863-1595; e-mail: dale_mierke@brown.edu.

[§] Department of Molecular Pharmacology, Brown University.

[||] Present address: BASF Bioresearch Corp., Worcester, MA 01605.

[⊥] M.P. and S.L. contributed equally to this work.

[#] Department of Chemistry, University of Pennsylvania.

[▽] Present address: Department of Drug Metabolism, Merck Research Laboratories, West Point, PA 19486.

[▼] Fox Chase Cancer Center.

[○] Present address: Incyte Pharmaceuticals, Inc., Palo Alto, CA 94304.

[●] Department of Chemistry, Brown University.

[1] Abbreviations: DTT, dithiothreitol; DG, distance geometry; DQF-COSY, double quantum filtered correlation spectroscopy; EDTA, ethylendiaminetetraacetate; IRMA, iterative relaxation matrix approach; Mamb, *m*-aminobenzoic acid; NMR, nuclear magnetic resonance; NOE, nuclear Overhauser enhancement; NOESY, nuclear Overhauser enhancement spectroscopy; mRR, mammalian ribonucleotide reductase; RMSD, root-mean-square deviation; ROESY, rotational-Overhauser enhancement spectroscopy; TOCSY, total-correlation spectroscopy.

10.1021/bi001323a CCC: $19.00 © 2000 American Chemical Society
Published on Web 09/13/2000

HPLC-purified to homogeneity, and characterized by mass spectrometry, as described in detail elsewhere (*10*). Assays of binding to mR1 were carried out using a competitive binding assay as described elsewhere (Pender et al., in preparation). Briefly, an FTLDADF−Sepharose column is equilibrated with mR1 and the peptide inhibitors, and the quantity of mR1 eluted is determined [by the Bradford (*12*) assay, using a bovine serum albumin standard]. The higher the affinity of an inhibitory ligand for mR1, the more mR1 is eluted. Simple equations permit calculation of the K_d of the candidate inhibitory ligand from the amount of eluted mR1. The sample for the NMR studies contained 40 μM mR1 and 2 mM Peptide 3 (ratio 1:50) in an aqueous solution (8% D_2O) containing 25 mM phosphate buffer, pH 7.0, 1.5 mM EDTA, 1.5 mM DTT, 15 mM $MgSO_4$, and 50 mM KCl. The sample containing only Peptide 3 was prepared identically.

NMR Spectroscopy. All NMR spectra were collected at 5 °C on a Bruker AVANCE spectrometer operating at 600 MHz and processed using Bruker XWIN-NMR software or NMRPipe (*13*). Peak volumes were measured with *Felix* (Molecular Simulations, Inc.). Chemical shifts were calibrated with respect to internal tetramethylsilane. The resonances of the peptide were assigned using DQF-COSY (*14*), TOCSY (*15, 16*), ROESY (*17, 18*), and NOESY (*19, 20*) spectra on the sample containing only Peptide 3. NOESY spectra were recorded on the mR1/Peptide 3 sample at mixing times of 45, 80, 100, 125, and 200 ms, to provide the input data for the full relaxation matrix calculations. All experiments used WATERGATE for water suppression (*21*).

Structure Refinement Calculations. To generate the starting ensemble for the full-relaxation matrix method, distance geometry (DG) calculations using a home-written program employing the random metrization method of Havel (*22*) were carried out. Proton−proton distances for the DG calculations were derived from the 125 ms NOESY spectrum, using as a reference the cross-peak between β-protons of Asp^6 (1.78 Å), and adjusted by ±10% to produce the upper and lower distance restraints. At this stage, pseudo-atoms were used for aromatic protons and for methylene protons that could not be stereospecifically assigned. The five structures with the lowest penalty function from the DG calculations were retained for the ensemble-based IRMA calculations (*23*−*25*).

The restraints were given as cross-peak volumes at the five different mixing times collected, with a ±20% adjustment. Each of the structures was soaked in a periodic box of water and energy-minimized using DISCOVER (Molecular Simulations, Inc.). IRMA was run with this initial ensemble of structures, generating an updated list of restraints aimed to produce structures in better agreement with the NOE intensities. After every iteration of IRMA, extensive energy minimization and molecular dynamics were carried out, applying the updated set of restraints. At this stage, each individual structure was removed from the ensemble and the agreement with the NOE intensities of the reduced ensemble examined. If the NOE penalty or the NOE *R*-factor (*26*) did not increase, the structure was not included in the next iteration, following the standard protocol for cross-validation (*27*). Following this protocol, the ensemble was reduced to three structures. The IRMA-based refinement calculations were repeated until the NOE *R*-factor did not further decrease for two iterations. The coordinates have been deposited in the Protein Data Bank (accession code 1foz).

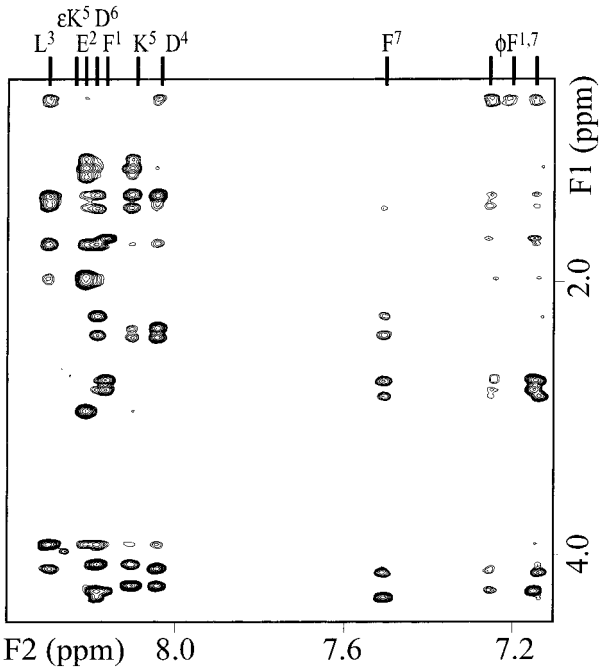

FIGURE 1: Expanded portion (fingerprint region) of one of the NOESY spectra (mixing time of 125 ms, temperature 5 °C), collected of Ac-F-c[ELDK]-DF with mR1 (see text for experimental conditions). The assignment of the amide protons is given above the spectrum (ϵ denotes the amide proton of the E−K lactam bridge).

RESULTS AND DISCUSSION

Conformation of AcF-c[ELDK]-DF-OH Free and Bound to mR1. Peptide 3, in the absence of mR1, displays only very weak NOEs in the NOESY spectrum (mixing time 200 ms), as expected given the small size of the molecule (MW 937) and the observation temperature (5 °C). In addition to the expected intraresidue and sequential NOEs, $i,i+3$ NOEs are observed between E^2 and K^5, arising from the lactam ring. An additional E^2-Hγ−D^4-HN cross-peak is present, although of very weak intensity. Amide−amide, HN(i)−HN($i+1$) NOEs are observed between residues 2/3, 3/4, 5/6, and 6/7. The collection of a ROESY spectrum (mixing time 200 ms) did not provide any evidence for additional interproton interactions.

By contrast, in the presence of mR1, Peptide 3 displays 68 unambiguous NOEs which were utilized in the structure refinement calculations. In comparison to the free peptide, the cross-peaks are visibly more intense at each of the mixing times (45−200 ms) employed and the resonances are significantly broader, as expected from the association to mR1. A representative NOESY spectrum, with a mixing time of 125 ms, is illustrated in Figure 1. The central turn, favored by the E^2−K^5 lactam bridge, is very well-defined by the weak K^5-HN to E^2-Hα and -Hβ and the medium/strong D^4-HN,E^2-H$\alpha,\beta,\gamma,\delta$ cross-peaks. The side chains as well adopt a preferred conformation described by a large number of short-range NOEs. In particular, the aromatic moieties of F^1 and F^7, residues known to be essential for activity, show contacts with L^3 and K^5, respectively. Sequential amide NOEs HN(i)−HN($i+1$) are present between residues 3−4, 6−7, and possibly 4−5 (the last one is ambiguous, given its proximity

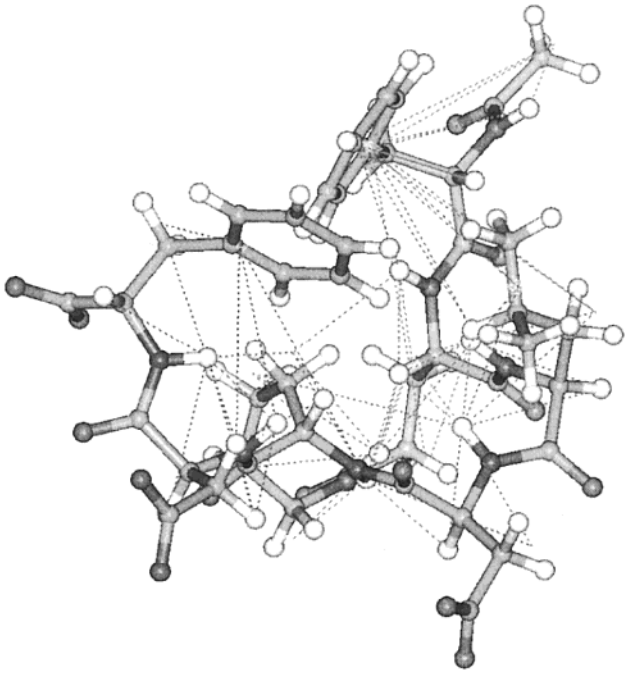

FIGURE 2: Illustration of the transferred NOEs measured for Ac-F-c[ELDK]-DF while bound to mR1. The NOEs are displayed (dotted lines) on one of the structures from the ensemble-based IRMA calculations.

Table 1: Dihedral Angles of the Two Structures of Ac-F-c[ELDK]-DF While Bound to the R1 Subunit of mRR As Determined by Transferred NOEs[a]

residue	ϕ	ψ	χ_1	χ_2	χ_3	χ_4
F^1	72, **−68**	173, **−53**	−110	−98		
E^2	72	55	−167, **−42**	79, **−66**		
L^3	−86	−38	64	94		
D^4	160	76	−179	73		
K^5	−85	106	62, **−60**	20, **156**	−71, **65**	−42, **53**
D^6	−90	−30	−174	73		
F^7	−54	−	−50	−88		

[a] Dihedral angles, which vary by more than 10° in the second structure, are given (boldface).

to the diagonal, and was therefore not utilized in the calculations). The density of NOE-based restraints for this small cyclic peptide is illustrated in Figure 2, using one of the resulting structures from the refinement calculations.

The structure refinement of Peptide 3 was carried out using an ensemble-based iterative relaxation matrix approach (IRMA) as developed by Kaptein and co-workers (*23*−*25*). The full-relaxation matrix approach accounts for the possibility of spin-diffusion in the build-up of the transferred NOEs. The utilization of an ensemble of molecules for the structure refinement (in contrast to employing a single structure and repeating the calculation numerous times) has been shown to be extremely valuable, particularly for peptides (*28*, *29*). The IRMA calculations resulted in three structures adopting two slightly different conformations (population weighted in a ratio of 2:1) which were consistent with the NOE intensities. The dihedral angles are given in Table 1. The ϕ,ψ values for D^4 and K^5 are different from those typically observed for proteins, a situation not uncommon for constrained, cyclic peptides. The structures differ in the backbone conformation of the exo-cyclic F^1 and in the orientation of the side chains of E^2 and K^5, which are

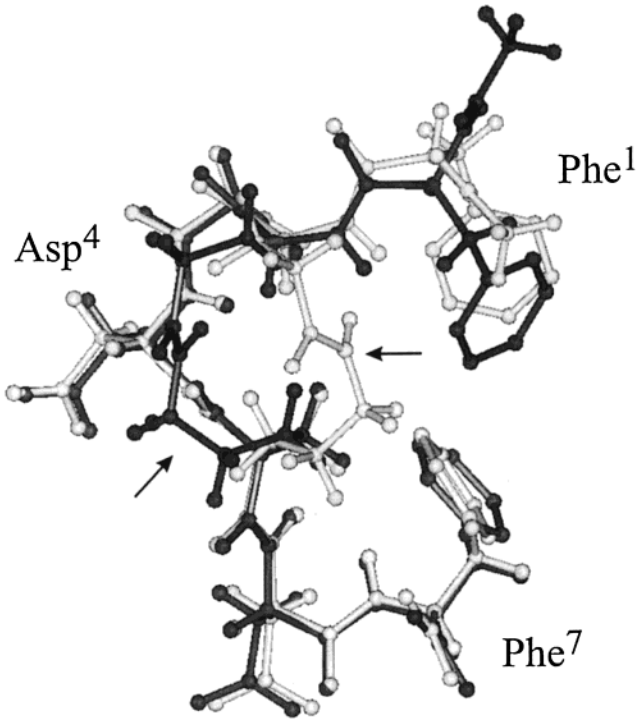

FIGURE 3: Superposition of the two different conformations observed for Ac-F-c[ELDK]-DF while bound to mR1 as determined by transferred NOEs. The different backbone conformations of F^1 and the alternative arrangements of the lactam side chains (denoted by arrows) are illustrated. The side chain of L^3 is not displayed for clarity. The conformation of the remainder of the molecule is very similar (an RMSD of 0.54 Å).

involved in the lactam ring system (Table 1). Despite these differences, the topological displays of the backbone and side chains are very similar, as depicted in Figure 3. The RMSD of the backbone atoms of the two structures, including F^1, is 0.54 Å.

Both structures of mR1-bound Peptide 3 are very amphipathic. The clustering of the side chains of F^1, L^3, and F^7, as well as of the *N*-acetyl terminus, provides a hydrophobic patch, dominating half of the molecule. On the opposing side, the side chains of D^4 and D^6, plus the C-terminus, form a negatively charged surface. The carbonyl groups of the lactam bridge, K^5, and D^6 all project in this same direction, adding to the negatively charged nature of this half of the molecule. The amphipathic character of the structure is illustrated in Figure 4.

The hydrophobic and hydrophilic faces of the molecule both seem to be important for overall activity. Replacement of either L^3 (Peptide 4) or D^4 (Peptide 5) with alanine leads to a dramatic drop in activity in each case, with the replacement of D^4 being more dramatic (Table 2). These results closely parallel substitution effects seen in the linear Peptide 1 (*7*, *8*). Interestingly, the effects do not appear to be additive, as simultaneous substitution of both L^3 and D^4 with alanine yields a cyclopeptide (Peptide 6) with activity similar to that of Peptide 5. Replacement of both L^3 and D^4 with *m*-aminobenzoic acid (Peptide 7) also results in very low binding affinity.

The observation of two conformations, which vary in the orientation of the lactam bridge, may indicate that this region is flexible while associated with the subunit or that these two orientations are both allowed bound conformations. The

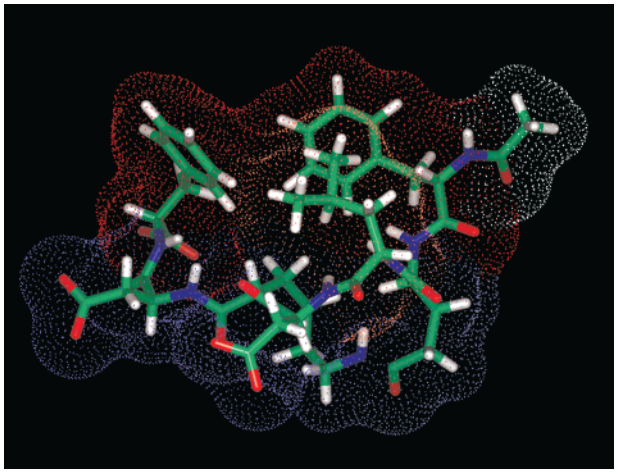

FIGURE 4: Structure of the favored conformer of Ac-F-c[ELDK]-DF while bound to mR1. The hydrophobicities (red, hydrophobic; blue, charged) of the amino acids are depicted in the coloration of the van der Waals surface (dots). The carbonyl groups of K^5 and D^6, the side chains of D^4 and D^6, and the C-terminus of the peptide all project in one direction (bottom of figure), opposite of the side chains of F^1, L^3, and F^7 (top of figure). The result is a very amphipathic molecule.

finding of two members of the ensemble adopting the first conformation, and one adopting the second conformation, may suggest that the first is favored. The lactam bridge, in addition to introducing conformational constraint and inducing specific arrangement of the side chains, may be interacting with the subunit as well. In our recent study (*10*), Peptide 3, containing an 18-membered lactam ring, had superior binding activity to mR1 (2.5-fold) than cyclopeptides with 16- and 17-membered rings, while the cyclopeptide with a 15-membered ring system bound with substantially reduced affinity. The observation that the larger ring systems are more active may imply that some flexibility in ring conformation is required. This would be consistent with the two conformations observed in this study.

Previously we reported a Monte Carlo conformational search in gas-phase for Peptide 3, which yielded low energy structures containing several intramolecular hydrogen bonds involving the lactam group (*10*). Interestingly, the structure of Peptide 3 when bound to mR1 adopts a completely different conformation, displaying no internal hydrogen bonds. Most of the amide and carbonyl groups are projecting outward, away from each other and the core of the peptide, and available as potential donors and acceptors for intermolecular hydrogen bonds with the mR1 subunit. The closest approach (3.1 Å) of a carbonyl and amide proton within the structure of Peptide 3 bound to mR1 is between the HN of D^6 and the CO of D^4.

Comparison of AcF-c[ELDK]-DF-OH and AcFTLDADF-OH Bound to mR1. Since both Peptides 1 and 3 bind to the same site in mR1, the structures of these molecules in the bound form, as determined by transferred NOEs, provide important insight into which structural features are critical for such binding. Similarities in the two structures should define features that must be maintained, while differences should highlight regions that can be further manipulated to confer higher affinity for mR1 and, by extension, higher potency to peptide and peptidomimetic inhibitors of mRR.

A comparison of the NOEs observed for the linear and cyclic molecules reveals several important similarities. For example, the NOE pattern involving F^1 and F^7 for Peptide 3 is strikingly similar to the one observed for the linear Peptide 1 while bound to mR1 (*9*). A number of NOEs between the side chains of F^1 and L^3 are observed at the N-terminus of both peptides. Similarly, at the C-terminus, NOEs between F^7 and K^5 (or A^5 for Peptide 1) are found for both inhibitors. In fact, the arrangement of many of the amino acids is similar in the mR1-bound conformations of Peptides 1 and 3. Structure−function studies on the linear peptide (*7*) (Pender et al., in preparation) indicate the importance for binding to mR1 both of the F^1, L^3, D^4, and F^7 side chains, and of the *N*-acyl and C-terminal carboxylate termini. Superimposing the side chain atoms of F^1, L^3, D^6, and F^7 (Figure 5) results not only in a reasonably good overlap of the three hydrophobic residues but also in similar orientations of D^6 and of the *N*-acetyl and anionic carboxylate termini in both the linear and cyclic peptides. This superposition produces an RMSD of 2.2 Å, which, given the large number of degrees of freedom associated with the side chains (e.g., χ_1, χ_2), is surprisingly small. Thus, lactam cyclization stabilizes the topological display observed for the termini and most of the side chains of bound linear peptide.

Table 2: Dissociation Constants from mR1

peptides	dissociation constant, μM
Ac-FTLDADF-OH (1)	10 ± 2
Ac-YTLDADF-OH (2)	150[a]
Ac-F-c[ELDK]-DF-OH (3)	4 ± 1
Ac-F-c[EADK]-DF-OH (4)	30 ± 5
Ac-F-c[ELAK]-DF-OH (5)	120 ± 10
Ac-F-c[EAAK]-DF-OH (6)	140 ± 10
Ac-F-c[E(Mamb)K]-DF-OH (7)	>200

[a] Reference (*8*).

There are, however, two important differences between the conformations of the two bound peptides that are particularly pertinent for residues D^4 and F^7. Direct evidence for the importance of a polar residue at position 4 comes from structure−function studies showing that while D^4 to N^4 substitution in Peptide 1 is well tolerated (*7*), D^4 to A^4 substitution in both Peptides 1 (*7*) and 3 (Table 2) leads to a large decrease in binding affinity to mR1. Despite this similarity, the D^4 side chain has a totally different orientation in the two peptides, indicating that the effects of D^4 to A^4 substitution in Peptides 1 and 3 must reflect the loss of different interactions with mR1. The difference in orientation is most evident in the relative topological display of the side chains of D^4 and D^6. As detailed above, both of the side chains are projecting in the same direction in Peptide 3, forming part of a negatively charged face. In contrast, in the linear peptide these amino acids project in opposite directions. Examination of the ϕ,ψ values of D^4 and A^5 (or K^5) for Peptides 1 and 3 reveals an approximately 180° rotation about D^4. This difference, and indeed the unusual ϕ,ψ values observed for D^4 in Peptide 3 (160°,76° while values of −128°,−49° are observed for the linear peptide), can be directly attributed to the cyclization of the two L-amino acids at positions 2 and 5.

The second difference is in the orientation of F^7. Although the F^7 side-chain orientation is not well-defined in the structure of bound Peptide 1 (*9*), it is nevertheless clear that it is oriented away from the core structure, leaving it free to insert into a relatively deep cavity on the mR1 surface (*30*)

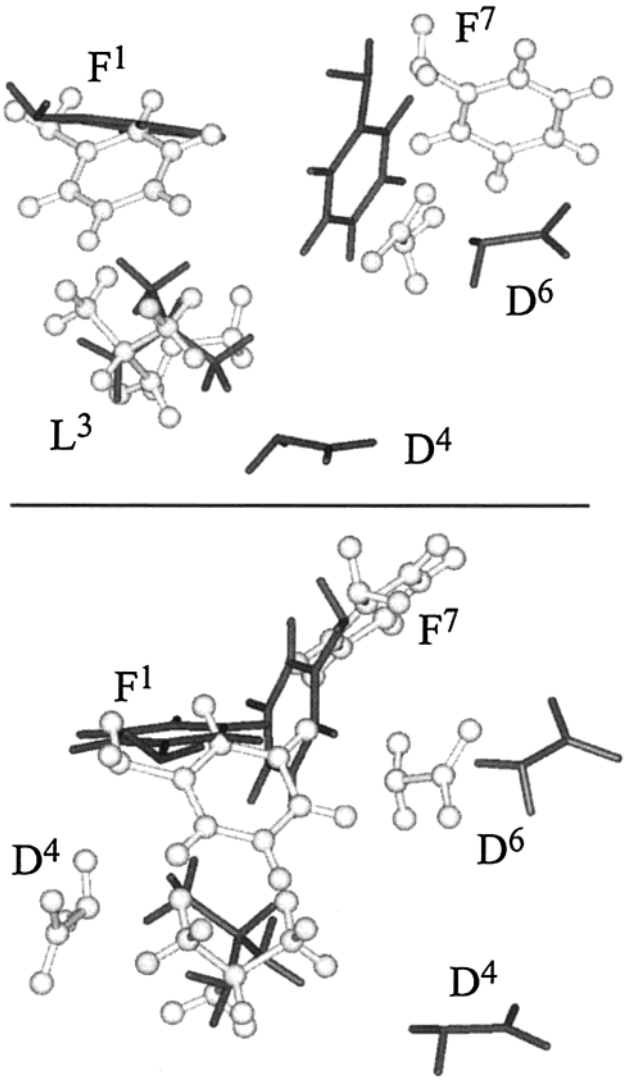

FIGURE 5: Superposition of the structures of Ac-F-c[ELDK]-DF (dark lines) and Ac-FTLDADF (light ball-and-sticks) while bound to mR1 (two views rotated by 90°). The heavy atoms of the side chains of F^1, L^3, D^6, and F^7 were used in the superposition. With the exception of D^4, all of the common side chains of the two peptides are similarly arranged.

which we denote the F^7 subsite. The available evidence (Pender et al., in preparation) strongly suggests that the binding of the F^7 side chain to this subsite contributes significantly to the binding energy of the association of mR2 C-terminal peptides with mR1. By contrast, in bound Peptide 3, the F^7 side chain turns into the core of the peptide (Figure 4), which, while extending the hydrophobic patch that also includes the *N*-acetyl terminus and the side chains of F^1 and L^3, drastically limits the extent to which this side chain can insert into the F^7 subsite. The fact that cyclic Peptide 3 binds to mR1 even more tightly than linear Peptide 1 suggests that the binding energy obtained through an increased interaction with the larger hydrophobic patch in Peptide 3 more than offsets the binding energy lost through poor insertion into the F^7 subsite.

The similarities and differences noted for Peptides 1 and 3 lead to the following working model for the design of high-affinity inhibitors of mRR. Both the hydrophobic patch, formed by the *N*-acetyl group and the triad of hydrophobic residues F^1, L^3, and F^7, and the anionic cluster, formed by the D^4 and D^6 side chains and the carboxyl terminus, appear to make important interactions with mR1, and each should be retained if not extended. In addition, structures that retain the hydrophobic patch but also have the ability to strongly interact with the F^7 subsite should have increased affinity for mR1. Modified forms of Peptide 3 having this potential are currently under active consideration. Further, as the cyclic peptide backbone may itself not be a crucial binding determinant, molecular scaffolds maintaining the arrangement of the important side chain and terminal groups discussed above also merit exploration.

Recently, Tanaka et al. (*31*) reported a p53-dependent R2 gene, *p53R2*, whose product: (a) is localized in the nucleus, (b) is thought to be important for the urgent supply of dNTPs for DNA repair, (c) is 80% identical with cytoplasmic mR2, and (d) has an identical R2 C-terminal heptapeptide. As yet unknown is whether there is a corresponding nuclear R1, distinct from cytoplasmic mR1. If so, it will clearly be of interest to explore possible differences in the interaction of peptide inhibitors with each R1 form, since, as pointed out by Lozano and Elledge (*32*), specific inhibition of cytoplasmic RR might allow repair synthesis in wild-type cells via p53R2 expression, while shutting off synthesis in p53-mutant tumors lacking p53R2.

REFERENCES

1. Cory, J. G. (1988) *Adv. Enzyme Regul. 27*, 437−455.
2. Beitler, J. J., Smith, R. V., Haynes, H., Silver, C. E., Quish, A., Kotz, T., Serrano, M., Brook, A., and Wadler, S. (1998) *Invest. New Drugs 16*, 161−169.
3. Stubbe, J. (1990) *J. Biol. Chem. 265*, 5329−5332.
4. Fontecave, M., Nordlund, P., Eklund, H., and Reichard, P. (1992) *Adv. Enzymol. Relat. Areas Mol. Biol.*, 147−183.
5. Sjoeberg, B.-M. (1995) *Nucleic Acids Mol. Biol. 9*, 192−224.
6. Hamann, C. S., Lentainge, S., Li, L. S., Salem, J. S., Yang, F. D., and Cooperman, B. S. (1998) *Protein Eng. 11*, 219−224.
7. Fisher, A., Yang, F. D., Rubin, H., and Cooperman, B. S. (1993) *J. Med. Chem. 36*, 3859−3862.
8. Fisher, A., Laub, P. B., and Cooperman, B. S. (1995) *Nat. Struct. Biol. 2*, 951−955.
9. Laub, P. B., Fisher, A. L., Furst, G. T., Barwis, B. A., Hamann, C. S., and Cooperman, B. S. (1997) Nmr, 26 Structures, Protein Databank Id: 1AFT, MMDB Id: 5993.
10. Liehr, S., Barbosa, J., Smith, A. B., III, and Cooperman, B. S. (1999) *Org. Lett. 1*, 1201−1204.
11. Yang, F. D., Spanevello, R. A., Celiker, I., Hirschmann, R., Rubin, H., and Cooperman, B. S. (1990) *FEBS Lett. 272*, 61−64.
12. Bradford, M. M. (1976) *Anal. Biochem 72*, 248−254.
13. Delaglio, F., Grzesiek, S., Vuister, G. W., Zhu, G., Pfeifer, J., and Bax, A. (1995) *J. Biomol. NMR 6*, 277−293.
14. Rance, M., Sørensen, O. W., Bodenhausen, G., Wagner, G., Ernst, R. R., and Wüthrich, K. (1983) *Biochem. Biophys. Res. Commun. 117*, 458−479.
15. Braunschweiler, L., and Ernst, R. R. (1983) *J. Magn. Reson. 53*, 521−528.
16. Bax, A., and Davis, D. G. (1985) *J. Magn. Reson. 65*, 355−360.
17. Bothner-By, A. A., Stephens, R. L., Lee, J., Warren, C. D., and Jeanloz, R. W. (1984) *J. Am. Chem. Soc. 106*, 811−813.
18. Bax, A., and Lerner, L. (1986) *J. Magn. Reson. 69*, 375−380.
19. Macura, S., Huang, Y., Suter, D., and Ernst, R. R. (1981) *J. Magn. Reson. 43*, 259−281.
20. Jeener, J., Meier, B. H., Bachmann, P., and Ernst, R. R. (1979) *J. Chem. Phys. 71*, 4546−4553.
21. Piotto, M., Saudek, V., and Sklenar, V. (1992) *J. Biomol. NMR 2*, 661−665.
22. Havel, T. F. (1991) *Prog. Biophys. Mol. Biol. 56*, 43−78.

23. Boelens, R., Koning, T. M. G., and Kaptein, R. (1988) *Mol. Struct. 173*, 299.
24. Boelens, R., Koning, T. M. G., van der Marel, G. A., Van Boom, H., and Kaptein, R. (1989) *J. Magn. Reson. 82*, 290.
25. Bonvin, A. M., Rullmann, J. A., Lamerichs, R. M., Boelens, R., and Kaptein, R. (1993) *Proteins: Struct., Funct., Genet. 15*, 385−400.
26. Gonzales, C., Rullmann, J. A. C., Bonvin, A. M. J. J., Boelens, R., and Kaptein, R. (1991) *J. Magn. Reson. 91*, 659−666.
27. Brunger, A. T., Clore, G. M., Gronenborn, A. M., Saffrich, R., and Nilges, M. (1993) *Science 261*, 328−331.
28. Mierke, D. F., Kurz, M., and Kessler, H. (1994) *J. Am. Chem. Soc. 116*, 1042−1049.
29. Mierke, D. F. (1998) *J. Am. Chem. Soc. 120*, 10721−10723.
30. Uhlin, U., and Eklund, H. (1994) *Nature 370*, 533−539.
31. Tanaka, H., Arakawa, H., Yamaguchi, T., Shiraishi, K., Fukuda, S., Matsui, K., Takei, Y., and Nakamura, Y. (2000) *Nature 404*, 42−49.
32. Lozano, G., and Elledge, S. J. (2000) *Nature 404*, 24−25.

BI001323A